

Germanium microlasers on metallic pedestals

A Elbaz, M El Kurdi, A. Aassime, S. Sauvage, X. Checoury, I. Sagnes, C Baudot, F. Boeuf, Philippe Boucaud

▶ **To cite this version:**

A Elbaz, M El Kurdi, A. Aassime, S. Sauvage, X. Checoury, et al.. Germanium microlasers on metallic pedestals. APL Photonics, 2018. hal-02155862

HAL Id: hal-02155862
https://hal.science/hal-02155862

Submitted on 14 Jun 2019

HAL is a multi-disciplinary open access archive for the deposit and dissemination of scientific research documents, whether they are published or not. The documents may come from teaching and research institutions in France or abroad, or from public or private research centers.

L'archive ouverte pluridisciplinaire **HAL**, est destinée au dépôt et à la diffusion de documents scientifiques de niveau recherche, publiés ou non, émanant des établissements d'enseignement et de recherche français ou étrangers, des laboratoires publics ou privés.

Germanium microlasers on metallic pedestals

A. Elbaz,[1,2] M. El Kurdi,[1] A. Aassime,[1] S. Sauvage,[1] X. Checoury,[1] I. Sagnes,[1] C. Baudot,[2] F. Boeuf,[2] and P. Boucaud[1]

[1)] *Centre de Nanosciences et de Nanotechnologies, CNRS, Univ. Paris-Sud, Université Paris-Saclay, Bâtiment 220, Rue André Ampère, F-91405 Orsay, France*

[2)] *STMicroelectronics, 850 Rue Jean Monnet F-38920 Grenoble, France*

Strain engineering is a powerful approach in micro and optoelectronics to enhance carrier mobility, tune the bandgap of heterostructures or break lattice symmetry for nonlinear optics. The dielectric stressors and bonding interfaces used for strain engineering in photonics can however limit thermal dissipation and the maximum operation temperature of devices. We demonstrate a new approach for enhanced thermal dissipation with stressor layers by combining metals and dielectrics. The method is applied to the germanium semiconductor. All-around tensile-strained germanium microdisks have been fabricated with metallic pedestals. The transferred tensile strain leads to a germanium thin film with a direct bandgap. Under continuous wave optical pumping, the emission of the whispering gallery modes is characterized by a threshold and an abrupt linewidth narrowing by a factor larger than 2. The occurrence of stimulated emission is corroborated by modeling of the optical gain. This demonstrates lasing with pure germanium microdisks.

INTRODUCTION

Strain engineering is a well-known method to modify the material properties. In microelectronics, strain transfer is used to boost carrier mobility as demonstrated with silicon-based transistors or III-V based transistors.[1] In optoelectronics, strain was introduced to lift valence band degeneracy and lower the threshold of quantum well lasers.[2] Strain has also been introduced in silicon photonics to break the centrosymmetry of the silicon lattice, thus enabling second-order nonlinear optical processes.[3] Strain can be used to tailor the bandgap of semiconductors or manipulate the band offsets. Germanium is a very symptomatic example of the benefit that can be retrieved from strain engineering. Germanium is an indirect bandgap semiconductor with about 140 meV of energy difference between the zone-center Γ conduction band and the L conduction band. Γ and L energy bands have different deformation potential parameters.[4] Upon strain application, the energy difference between Γ and L can be controlled and, providing that high enough strain is applied, the semiconductor can even become direct bandgap. This situation can only be obtained when very large uniaxial (> 4 %) or biaxial ($>1.6\%$) tensile strains are applied. Different methods for strain transfer to germanium have thus been investigated. Patterning tensile-strained germanium into microbridges can enhance the tensile strain[5] and provide direct band gap germanium.[6,7] Nanomembrane fabrication of germanium has also been proposed.[8] Another approach consists in introducing stressor layers like dielectric silicon nitride. By depositing compressively strained silicon nitride, a tensile strain can be transferred into germanium when the silicon nitride is allowed to move freely.[9–11] To enhance the strain transfer, an all-around stressor approach has been proposed.[12] In the latter case, a stressor is present at the bottom, on top and on the edges of microstructures. This three-dimensional strain is obtained by bonding a strained germanium layer on a host substrate through a silicon oxide layer. Silicon oxide is known to have a poor thermal conductivity and the temperature of an all-around strained microstructure can rapidly increase significantly under optical pumping, thus degrading the performance of devices. A similar situation happens for suspended microbridges where thermal dissipation prevents lasing with the free-standing material.[13,14]

Lasing with group IV semiconductors is easier when a direct bandgap is present since the oscillator strength of direct bandgap transitions is larger than the one of indirect bandgap materials and a direct bandgap favors the zone centre electron population. For this reason,

alloying germanium with tin is a viable option, a concentration of tin around 10 % allowing one to obtain a direct bandgap semiconductor. Lasing with GeSn alloys has been recently demonstrated first in ridge lasers[15] and later in microdisks.[16] Under pulsed optical excitation, the maximum lasing temperature was 180 K. One drawback of alloying with tin is the decrease of the material quality with enhanced non-radiative recombinations. Moreover, GeSn alloys are deposited at low temperature ($<$ 400 °C) thus imposing stringent temperature maxima on back-end processing to avoid material degradation and tin precipitations.[16,17] Having pure germanium for a group IV laser is thus still highly desirable. Lasing with very lightly strained germanium has been reported but with very high excitation densities and close to samples breakdown.[18,19] Lasing has been reported with uniaxially strained germanium microbridges under pulsed optical pumping.[20] The applied strain was however far below the one needed to obtain a direct bandgap. In the latter case, thermal management was also limited by the oxide film on which the microbridges are attached. A better option would be to use direct bandgap germanium as obtained with all-around stressor layer approach.[12] So far, lasing was prevented with this all-around stressor approach because of poor thermal management induced by the intermediate oxide layer in the strained-germanium on oxide devices.

Here, we introduce a novel method to fabricate tensile-strained germanium microdisks by replacing the oxide pedestal with a metallic pedestal. The realization of a semiconductor-on-metal heterostructure is obtained by a selective wet etching between aluminum and germanium. With this approach, the germanium film can be fully strained by silicon nitride stressor layers and keeps a strongly optimized thermal dissipation thanks to the metallic pedestal. The metal pedestal does not degrade the quality factor of microresonators and we have measured linewidths as small as 0.35 nm at transparency, that corresponds to quality factors up to 5680, in strained germanium microdisks. Continuous wave (cw) lasing of germanium microlasers is reported for the first time with cw lasing around 2 μm. Laser emission is observed up to 80 K and narrow resonance peaks at least up to 140 K.

SAMPLE FABRICATION

Figure 1 (a) shows a schematic layout of the processed structure with its metal post. The starting heterostructure is a germanium film grown on a silicon-on-insulator substrate

(germanium thickness 850 nm). A silicon nitride layer, referred to as SiN in the following, that will become the bottom stressor layer, is first deposited on top of this structure (350 nm). The metal, aluminum, is deposited in an e-beam evaporator. A SiN diffusion barrier (100 nm) is then deposited by plasma-enhanced chemical vapor deposition.

This barrier blocks the diffusion of the gold into the aluminum during the bonding. The whole structure is then bonded on a Si handle substrate through metallic Au-Au bonding. The silicon-on-insulator substrate is then removed and the germanium layer is thinned to the required thickness (360 nm), removing the Ge/Si interface region where numerous defects are present. This step limits the non-radiative recombinations in germanium and enhance the radiative recombination efficiency. This step is described in more details in the supplementary. The thickness is sufficiently high to support TM-polarized modes in the microdisk. The structure is then processed by electronic lithography to fabricate microdisks by using plasma etching of the germanium and SiN. The choice of the metal for the post was dictated by the selectivity for underetching of the germanium microdisks. We have found that KOH has a high chemical selectivity between germanium and aluminum thus allowing to underetch aluminum without etching germanium. Once the metallic post, 700 nm thick, is defined, silicon nitride layer (-1.9 GPa stress, 600 nm) is deposited by plasma-enhanced chemical vapor deposition thus leading to an all-around strained microdisk on a metallic post. Figure 1 (b) shows a scanning electron microscope image of the fabricated microdisk on metal before the second layer deposition of SiN. We note that the all-around strained germanium supports annealing temperatures at least up to 500 °C as well as the metallic bonding.

RESULTS

Figures 2 (a) and (b) show the calculated trace of the strain field in the microdisk with a metallic pedestal. Figure 2 (a) corresponds to a layer plane cross-section in the middle of the germanium film while Fig. 2 (b) corresponds to a two-dimensional mapping. We have plotted the trace of the strain field since the energy difference between the Γ and L valleys is directly proportional to this parameter. Interestingly, the metal pedestal does not limit the strain transfer from the silicon nitride layers to the germanium. The Young modulus of the metal is equivalent to the one of the oxide (70 GPa). We can obtain an

equivalent biaxial strain field up to 1.7 % in the same range as previously reported.[12] The strain is larger at the edge of the microdisk where the whispering gallery modes are located. As germanium can become direct bandgap for biaxial strain larger than 1.67%,[21] direct bandgap germanium can be obtained with this method. The amplitude of the strain field was confirmed by photoluminescence measurements, as discussed later. Figures 2 (c) and (d) show the calculated temperature profile in the microdisk when the post is made of silicon oxide (c) or when the post is metallic (d). The temperature is calculated considering an 8 mW optical pumping with a ring excitation (10 μm outer diameter, 1 μm inner width) incident on the microdisk. The additional parameters considered for the modeling of strain field and temperature are given in the supplementary.

The temperature profile is strikingly different between both configurations. With oxide posts, the thermal diffusion is limited by the oxide thermal conductivity (0.13 W/(m K) at 15 K, 1.4 W/(m K) at room temperature). A temperature increase up to 310 K is obtained in the microdisk for a boundary substrate temperature of 15 K. On the contrary, the temperature rise is limited to 40 K with the metal post. For the investigated range, the temperature rise is linear as a function of the pump power. The exact temperature profile depends ultimately on excitation geometry, either annular excitation or single spot at the center or at the edge of the microdisk but the trend remains the same. Strained microdisks on metals provide thus an enhanced thermal management as compared to previous reports with oxide posts, and the progress brought by the metal pedestal explains the results discussed hereafter. We note that this improvement is not limited to the replacement of SiO_2 interface. The benzocyclobutadiene (BCB), frequently used for bonding of semiconductor heterostructures, has a thermal conductivity in the same range as the oxide layer (0.29 W/mK) and could as well be advantageously replaced by metal posts in some cases.

Figure 3 (a) shows the spectra of a 12 μm microdisk under cw optical pumping at 1.06 μm at low temperature (15 K). The pumping is done with a ring excitation (10 μm outer diameter, 1 μm width) using a combination of an axicon and objective lenses. This annular excitation allows one to deposit the energy at the location of whispering gallery modes on the edges of the microdisks and enhances the contrast between whispering gallery modes and background spontaneous emission that mostly comes from the disk center. The emission is collected from the top surface. As discussed below, this configuration is not optimal for the collection of the whispering gallery modes as these modes tend to radiate preferentially in

the layer plane. This configuration generally leads to a weak contrast between laser peaks and background spontaneous emission.[22,25] The contrast between whispering gallery modes and background spontaneous emission would be higher with side collection. Polarization-resolved emission would as well be possible with side collection.

Several features can be observed on Fig. 3 (a). At low excitation power, only a broad background spontaneous emission is observed with a maximum around 1.98 μm. This emission stems from the direct bandgap of the tensile-strained germanium with an equivalent biaxial tensile strain of 1.7 %, in agreement with the strain field calculation obtained by finite element modeling. With this tensile strain, germanium has a direct bandgap, the Γ valley being aligned with the L valley within a few meV. The large broadening of the emission results from the inhomogeneity of the strain field (See supplementary for the modeling of the photoluminescence spectrum). As the pump density is increased, resonant peaks are observed around the emission maximum and on the high energy side of the emission. These resonant peaks are attributed to whispering gallery modes. A calculation of the spectral positions of the whispering gallery modes in TM-polarization is presented in the supplementary. A large number of resonances are predicted with high-order radial modes and it is difficult to identify unambiguously the first-order radial modes. We note that high-order radial modes are not quenched in these structures since these modes do not overlap more significantly than first-order radial modes with the pedestal. Figures 3 (b) and (c) show a zoom of the emission around 1980 and 2030 nm, obtained by recording only one field on the array detector. There is a clear threshold for the resonant modes that are associated to the onset of lasing. Figure 3 (d) illustrates the dependence of the integrated intensity for three distinct modes at 1966, 1987 and 2036 nm as a function of the incident pump power. The threshold occurs around 5 mW i.e. 18 kW cm^{-2}, the threshold increasing when going to shorter wavelength. This increase is due to the fact that more carriers are needed to reach population inversion at high energy, as confirmed by optical gain modeling. Simultaneously, there is a significant linewidth narrowing as shown in figure 3 (d) which is another signature of the stimulated emission process. A reduction by a factor larger than 2 is observed as expected from Schawlow-Townes equations for the transition between incoherent emission to coherent emission (See supplementary).

DISCUSSION

The combination of threshold and linewidth narrowing by a factor greater than 2 are evidences of lasing in these strained microdisks under continuous wave optical excitation. As discussed below, the occurence of stimulated emission is as well corroborated by the modeling of the optical gain. Several features specific of microdisk lasing need to be emphasized.

These threshold values are significantly smaller than the best results reported for GeSn microdisks and in the latter case for pulsed excitation. We emphasize that for biaxially-strained germanium, stimulated gain is expected for Transverse-Magnetic polarization, i. e. for an electric field perpendicular to the layer plane. The spontaneous emission in TE polarization coming from the whole volume of the disk, including the center of the microdisk, is more efficiently collected and continues to increase even when lasing is achieved in TM-polarization. The contrast between stimulated emission and spontaneous emission is thus not as strong as the one observed in standard cavities since carrier clamping and spontaneous emission clamping only concerns a fraction of the global emission. The ratio between the whispering gallery mode amplitude and the background emission is shown in figure S6 in the supporting information. It highlights the clear dynamics for the whispering gallery modes around the threshold.

The smallest linewidth is 0.35 nm (spectrometer resolution 0.2 nm) for the mode at 1987 nm, measured after the sharp decrease of the linewidth, i.e. close to transparency. Assuming that there is no stimulated emission, it corresponds to quality factors up to 5680. Observing such high quality factors at the peak of the emission of the strained germanium, i.e where the absorption becomes significant, is only possible if the bulk material absorption is quenched. The quality factors are probably limited by the roughness scattering at the microdisk sidewalls (see supplementary). We note that these quality factors are larger than those reported in Ref.[16] with GeSn microdisks (Q $\sim$ 200-400) or in Ref.[26] with microbridges (Q $\sim$ 2000). The higher quality factors contribute to the reduction of the threshold as the excess excitation energy needed between transparency and lasing onset is inversely proportional to the Q factor.[27] As seen in Figures 3 (b) and (c), some lines consist of nearly-degenerate modes whose splitting is more obviously observed at high pump energy. We have not considered these modes to extract the linewidth narrowing. Note that we do not observe such linewidth narrowing for the whispering gallery modes located on the indirect bandgap spectral range

of microdisks with lower strain (See supplementary). This observation reinforces the evidence of lasing for the microdisks with metallic pedestals. The linewidth narrowing tends to saturate at large pump powers. Such behavior has already been observed in other microdisk systems.[23] Several mechanisms like an excess noise factor from incomplete population inversion, the Petermann factor that relates the excess noise to mode non-orthogonality and the Henry factor that relates the phase noise to amplitude might explain this saturation in linewidth narrowing that does not fully follow the canonical Schawlow-Townes relation.[24]

There is no strong mode competition in these strained microdisks and we attribute this feature to the large inhomogeneous broadening of the emission due to strain field variation in the bulk semiconductor and to carrier diffusion as well. The situation differs from the textbook scenario with a pure homogeneously-broadened emission.

We have investigated the temperature dependence of the stimulated emission in the microdisks. The spontaneous emission of the germanium layer was first investigated as a function of temperature. The integrated emission is roughly constant from room temperature to low temperature in these all-around strained microdisks, as described in the supplementary section. It indicates that the non-radiative lifetime is almost constant as a function of the temperature. We note that the photoluminescence amplitude is a complex function of the band structure (direct or indirect), the evolution of the non-radiative recombination paths vs. temperature, the presence of defects like dislocations[28], the diffusion length of carriers and their redistribution in strained regions[29], and surface recombinations. Figure 4 (a) shows the optical spectra for a fixed incident energy density of 29 kW cm^{-2} (8 mW incident power). It corresponds to a carrier density of 2.5×10^{18} cm^{-3} at low temperature for a 1 ns carrier lifetime, 2 % being in the Γ valley. As seen, the resonant modes are observed up to 140 K with a continuous wave pumping. We have performed the same measurements as in Figure 3 at 80 K and threshold and linewidth narrowing are as well observed (See supplementary). From figure 4, we postulate that lasing is obtained up to 140 K but we did not perform a systematic study at this temperature. If we account for the temperature increase in the disk following Figure 2 (d), it indicates that stimulated emission could be observed up to 180 K.

We have modeled the net optical gain in strained germanium at 2 μm following Ref.[30]. The free carrier absorption and intervalence band absorption was considered according to Refs.[31,32]. Three parameters play a significant role for the gain amplitude: the energy difference between Γ and L valleys, the homogeneous broadening and the temperature of

the microdisk. An homogeneous broadening of 25 meV was considered and a Γ-L energy difference of 0 meV, as obtained from strain modeling with an equivalent biaxial strain of 1.7%. These parameters provide a good fit with the photoluminescence recombination.

As shown in Fig. 4 (b), the modeling indicates that a theoretical net optical gain is expected for temperatures up to 230 K. This is consistent with the experimental result: the temperature of 140 K is the one in the cryostat and there is roughly a 40 K temperature increase for 8 mW pump power as illustrated in Fig. 2. A better agreement could even be obtained by inserting a dependence of the homogeneous broadening as a function of the temperature. We note that on Fig. 3 (b), there is hardly no shift of the whispering gallery mode resonances, as compared to oxide pedestals, confirming the weak temperature increase in the disk. The thermo-optic effect remains nonetheless detrimental to the stimulated emission. As the pump power is increased, the temperature rise counterbalances the expected increase of gain and limits the dynamics range of the resonant emission, i.e. the stimulated emission tends to level off. We note that the modeling predicts an increase of the threshold by a factor around 1.5 from 15 K to 80 K, as experimentally observed. With the considered parameters, optical gain is only predicted for TM-polarization for the investigated optical densities. The modes observed in Fig. 3 are thus TM-polarized and their large numbers are correlated with the calculation of their spectral position as shown in the supplementary.

To increase the operation temperature, a larger population of electrons in the Γ valley is required. This could be obtained by increasing the energy difference between the Γ and L valleys with an increase of the applied strain. A decrease of the non-radiative recombinations by optimizing the passivation and etching recipes could as well decrease the threshold and consequently decrease the temperature rise in the microdisk. The temperature rise might be lower under pulsed condition if the pulse time separation is larger than about 10 μs in order for the microdisk to thermalize between each pulse. We emphasize that lasing is obtained here thanks to the metallic pedestal. With an oxide post, the temperature rise with 29 kW cm^{-2} would be of 310 K, see Figure 2 (c), thus prohibiting the observation of lasing.

CONCLUSION

In conclusion, we have demonstrated a new approach to fabricate microlasers with all-around strained layers. The introduction of metallic posts has significantly improved the

thermal management without degrading the mechanical and optical properties of micro-lasers. The improvement in thermal management has led to the observation of lasing under continuous wave excitation in all-around strained microdisks with pure germanium and a direct bandgap. The combination of metal and dielectric heterostructures is not limited to microdisk topology and could be applied as well to ridge heterostructures and to integrated photonics with strained layers. The metal pedestal is also appropriate for electrical injection.[33]

SUPPLEMENTARY MATERIAL

The supplementary material consists of height different sections. The first section describes and models the effect of the strain homogeneity on the photoluminescence spectrum. The second section details the dependence of the photoluminescence as a function of temperature. The third section describes the experimental results on weakly-strained germanium where no lasing effect is observed. The fourth section provides more information on the fabrication processes. The fifth section gives the parameters used for the microdisk temperature modeling and provides a modeling of the whispering gallery modes for the all-around strained germanium microdisks. The sixth section shows the ratio between the whispering gallery mode amplitude and the background emission. The seventh section shows the measurements at 80 K. The last section consists in a table that summarizes the criteria expected for laser assessment. The threshold effect is once again emphasized in a specific figure.

ACKNOWLEDGMENTS

We acknowledge support from the RENATECH network and from ANRT for CIFRE grant.

FIGURE CAPTIONS

Figure 1. (a) Schematics description of the different processing steps. (1) germanium was first grown on a silicon-on-insulator substrate by chemical vapor deposition. The germanium-on-silicon wafer is covered by a silicon nitride film, followed by a metal film and bonded on a host silicon handle substrate. (2) The silicon substrate is removed and the germanium film is thinned to a thickness of 360 nm. Details on the thinning process are given in the supplementary (3) The microdisks are defined by electronic lithography and plasma etching. (4) A selective wet etching is used to define the metal post. A second silicon nitride film is deposited thus leading to an all-around strained structure. The deposition on the bottom surface is weak (1/10 of the top surface and 1/5 on the pedestal). (b) Example of a scanning electron microscopy image of a processed microdisk on a metal pedestal before the second SiN layer deposition.

Figure 2. (a) Trace of the strain field ($\varepsilon_{xx} + \varepsilon_{yy} + \varepsilon_{zz}$) calculated through the middle of the germanium layer in the layer plane. (b) Two-dimensional cross-section of the trace of the strain field in the whole structure as calculated by finite element. (c) Temperature profile of an all-around strained microdisk with a SiO_2 pedestal. The boundary limit set by the substrate temperature is 15 K. The incident energy density distributed in a ring at a 1064 nm wavelength is 29 kW cm^{-2}. The temperature reaches 326 K (d) Same temperature map but for a metal pedestal. The temperature only reaches 56 K with metal pedestal.

Figure 3. (a) Cw emission spectra at 15 K of a 12 μm diameter microdisk for different excitation densities. Water vapor absorption lines modulate the emission below 1940 nm. (b) Zoom of the emission around 1980 nm at 15 K. (c) Zoom of the emission around 2030 nm at 15 K. The black arrows indicate the three modes depicted in figure (d) and (e). (d) Integrated intensity for three different resonant modes at 1966, 1987 and 2036 nm. The background emission has been subtracted to obtain the mode integrated intensity. The threshold for lasing is around 5 mW, 18 kW cm^{-2}. The figures also show the linewidths for the three same modes as a function of the incident pump power. The increase above 10 mW for the 2036 nm mode is within the error bar.

Figure 4. Dependence of the emission as a function of the temperature. The modes are observed up to 140 K (cryostat temperature), the temperature in the disk is higher by roughly 40 K. (b) Gain modeling at 2 μm as a function of substrate temperature. Positive maximum gain is predicted up to 230 K. The maximum of the gain curve shifts at high energy when increasing pump power.

REFERENCES

[1] M. Chu, Y. Sun, U. Aghoram, and S. E. Thompson, Annu. Rev. Mater. Res. **39**, 203 (2009).

[2] D. Ahn and C. Shun-Lien, IEEE Journal of Quantum Electronics **24**, 2400 (1988).

[3] M. Cazzanelli, F. Bianco, E. Borga, G. Pucker, M. Ghulinyan, E. Degoli, E. Luppi, V. Véniard, S. Ossicini, D. Modotto, S. Wabnitz, R. Pierobon, and L. Pavesi, Nat Mater **11**, 148 (2012).

[4] J. Liu, D. D. Cannon, K. Wada, Y. Ishikawa, D. T. Danielson, S. Jongthammanurak, J. Michel, and L. C. Kimerling, Phys. Rev. B **70**, 155309 (2004).

[5] R. Geiger, J. Frigerio, M. J. Suess, D. Chrastina, G. Isella, R. Spolenak, J. Faist, and H. Sigg, Appl. Phys. Lett. **104**, 062106 (2014).

[6] D. S. Sukhdeo, D. Nam, J.-H. Kang, M. L. Brongersma, and K. C. Saraswat, Photon. Res. **2**, A8 (2014).

[7] A. Gassenq, K. Guilloy, G. Osvaldo Dias, N. Pauc, D. Rouchon, J.-M. Hartmann, J. Widiez, S. Tardif, F. Rieutord, J. Escalante, I. Duchemin, Y.-M. Niquet, R. Geiger, T. Zabel, H. Sigg, J. Faist, A. Chelnokov, V. Reboud, and V. Calvo, Appl. Phys. Lett. **107**, 191904 (2015).

[8] J. R. Sanchez-Perez, C. Boztug, F. Chen, F. F. Sudradjat, D. M. Paskiewicz, R. Jacobson, M. G. Lagally, and R. Paiella, Proceedings of the National Academy of Sciences **108**, 18893 (2011).

[9] A. Ghrib, M. de Kersauson, M. El Kurdi, R. Jakomin, G. Beaudoin, S. Sauvage, G. Fishman, G. Ndong, M. Chaigneau, R. Ossikovski, I. Sagnes, and P. Boucaud, Appl. Phys. Lett. **100**, 201104 (2012).

[10] G. Capellini, G. Kozlowski, Y. Yamamoto, M. Lisker, C. Wenger, G. Niu, P. Zaumseil, B. Tillack, A. Ghrib, M. de Kersauson, M. El Kurdi, P. Boucaud, and T. Schroeder, J. Appl. Phys. **113**, 013513 (2013).

[11] R. Millar, K. Gallacher, A. Samarelli, J. Frigerio, D. Chrastina, G. Isella, T. Dieing, and D. Paul, Opt. Express **23**, 18193 (2015).

[12] A. Ghrib, M. El Kurdi, M. Prost, S. Sauvage, X. Checoury, G. Beaudoin, M. Chaigneau, R. Ossikovski, I. Sagnes, and P. Boucaud, Advanced Optical Materials **3**, 353 (2015).

[13] J. R. Jain, A. Hryciw, T. M. Baer, D. A. B. Miller, M. L. Brongersma, and R. T. Howe, Nat Photon **6**, 398 (2012).

[14] P. Boucaud, M. El Kurdi, S. Sauvage, M. de Kersauson, A. Ghrib, and X. Checoury, Nat Photon **7**, 162 (2013).

[15] S. Wirths, R. Geiger, N. von den Driesch, G. Mussler, T. Stoica, S. Mantl, Z. Ikonic, M. Luysberg, S. Chiussi, J.-M. Hartmann, H. Sigg, J. Faist, D. Buca, and D. Grutzmacher, Nat Photon **9**, 88 (2015).

[16] D. Stange, S. Wirths, R. Geiger, C. Schulte-Braucks, B. Marzban, N. von den Driesch, G. Mussler, T. Zabel, T. Stoica, J.-M. Hartmann, S. Mantl, Z. Ikonic, D. Grutzmacher, H. Sigg, J. Witzens, and D. Buca, ACS Photonics **3**, 1279 (2016).

[17] S. Zaima, O. Nakatsuka, N. Taoka, M. Kurosawa, W. Takeuchi, and M. Sakashita, Science and Technology of Advanced Materials **16**, 043502 (2015).

[18] R. E. Camacho-Aguilera, Y. Cai, N. Patel, J. T. Bessette, M. Romagnoli, L. C. Kimerling, and J. Michel, Opt. Express **20**, 11316 (2012).

[19]R. Koerner, M. Oehme, M. Gollhofer, M. Schmid, K. Kostecki, S. Bechler, D. Widmann, E. Kasper, and J. Schulze, Opt. Express **23**, 14815 (2015).

[20]S. Bao, D. Kim, C. Onwukaeme, S. Gupta, K. Saraswat, K. H. Lee, Y. Kim, D. Min, Y. Jung, H. Qiu, H. Wang, E. A. Fitzgerald, C. S. Tan, and D. Nam, Nature Communications **8**, 1845 (2017).

[21]M. El Kurdi, M. Prost, A. Ghrib, S. Sauvage, X. Checoury, G. Beaudoin, I. Sagnes, G. Picardi, R. Ossikovski, and P. Boucaud, ACS Photonics **3**, 443 (2016).

[22]A. C. Tamboli, E. D. Haberer, R. Sharma, K. H. Lee, S. Nakamura, and E. L. Hu, Nature photonics **1**, 61 (2006).

[23]W. Fang, H. Cao, V. A. Podolskiy, and E. E. Narimanov, Opt. Express **13**, 5641 (2005).

[24]J. C. Pillay, Y. Natsume, A. D. Stone, and Y. D. Chong, Phys. Rev. A **89**, 033840 (2014).

[25]M. Athanasiou, R. Smith, B. Liu, and T. Wang, Scientific Reports **4**, 7250 (2014).

[26]J. Petykiewicz, D. Nam, D. S. Sukhdeo, S. Gupta, S. Buckley, A. Y. Piggott, J. Vučković, and K. C. Saraswat, Nano Lett. **16**, 2168 (2016).

[27]T. Baba and D. Sano, IEEE Journal of Selected Topics in Quantum Electronics **9**, 1340 (2003).

[28]F. Pezzoli, A. Giorgioni, D. Patchett, and M. Myronov, ACS Photonics **3**, 2004 (2016).

[29]D. Nam, D. S. Sukhdeo, J.-H. Kang, J. Petykiewicz, J. H. Lee, W. S. Jung, J. Vučković, M. L. Brongersma, and K. C. Saraswat, Nano Lett. **13**, 3118 (2013).

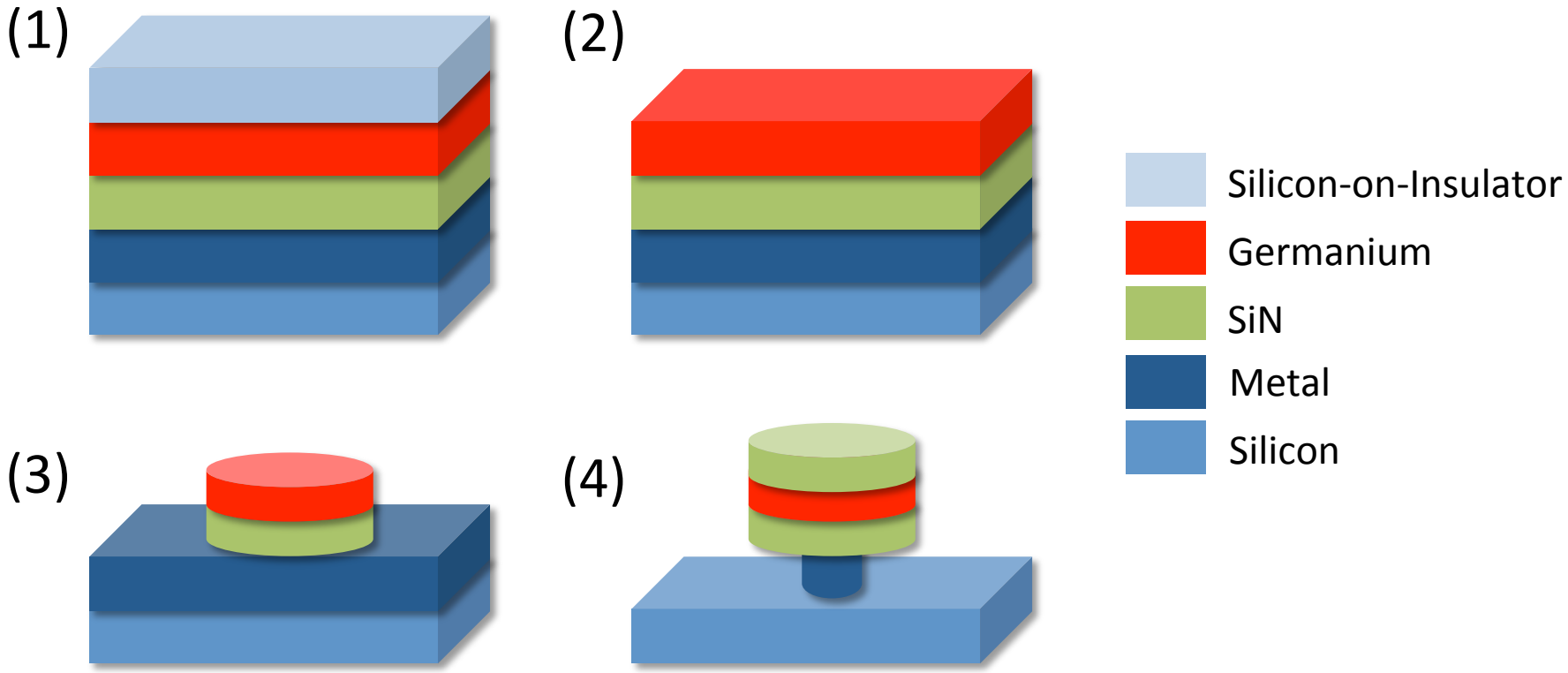
[30]M. El Kurdi, G. Fishman, S. Sauvage, and P. Boucaud, J. Appl. Phys. **107**, 013710 (2010).

[31]M. Nedeljkovic, R. Soref, and G. Mashanovich, IEEE Photonics Journal **7**, 1 (2015).

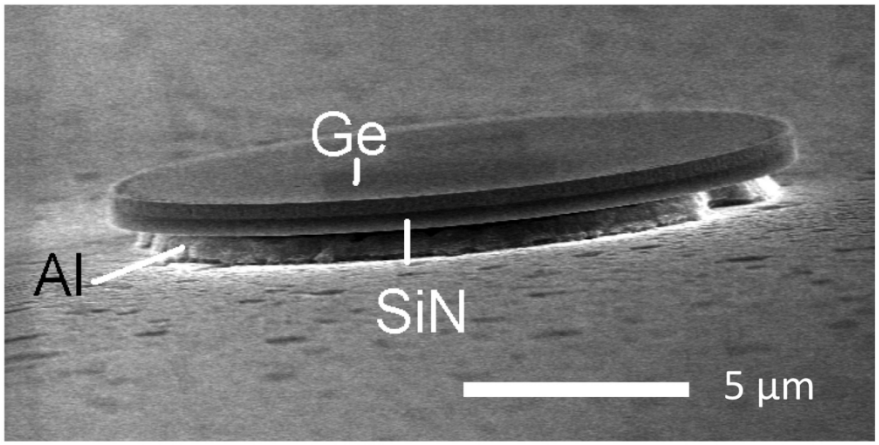
[32]P. Boucaud, M. El Kurdi, A. Ghrib, M. Prost, M. de Kersauson, S. Sauvage, F. Aniel, X. Checoury, G. Beaudoin, L. Largeau, I. Sagnes, G. Ndong, M. Chaigneau, and R. Ossikovski, Photon. Res. **1**, 102 (2013).

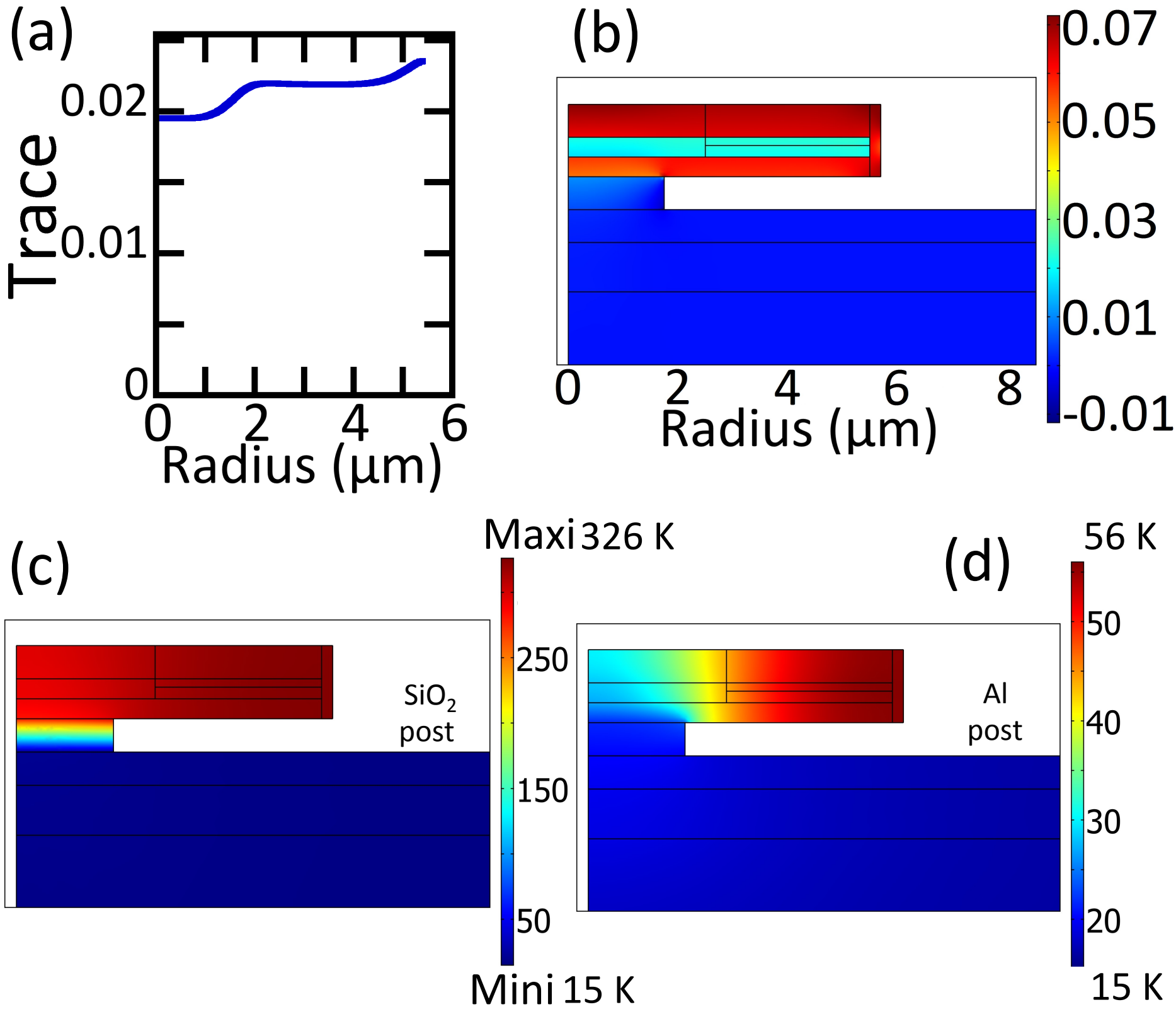
[33]M. de Kersauson, R. Jakomin, M. El Kurdi, G. Beaudoin, N. Zerounian, F. Aniel, S. Sauvage, I. Sagnes, and P. Boucaud, J. Appl. Phys. **108**, 023105 (2010).

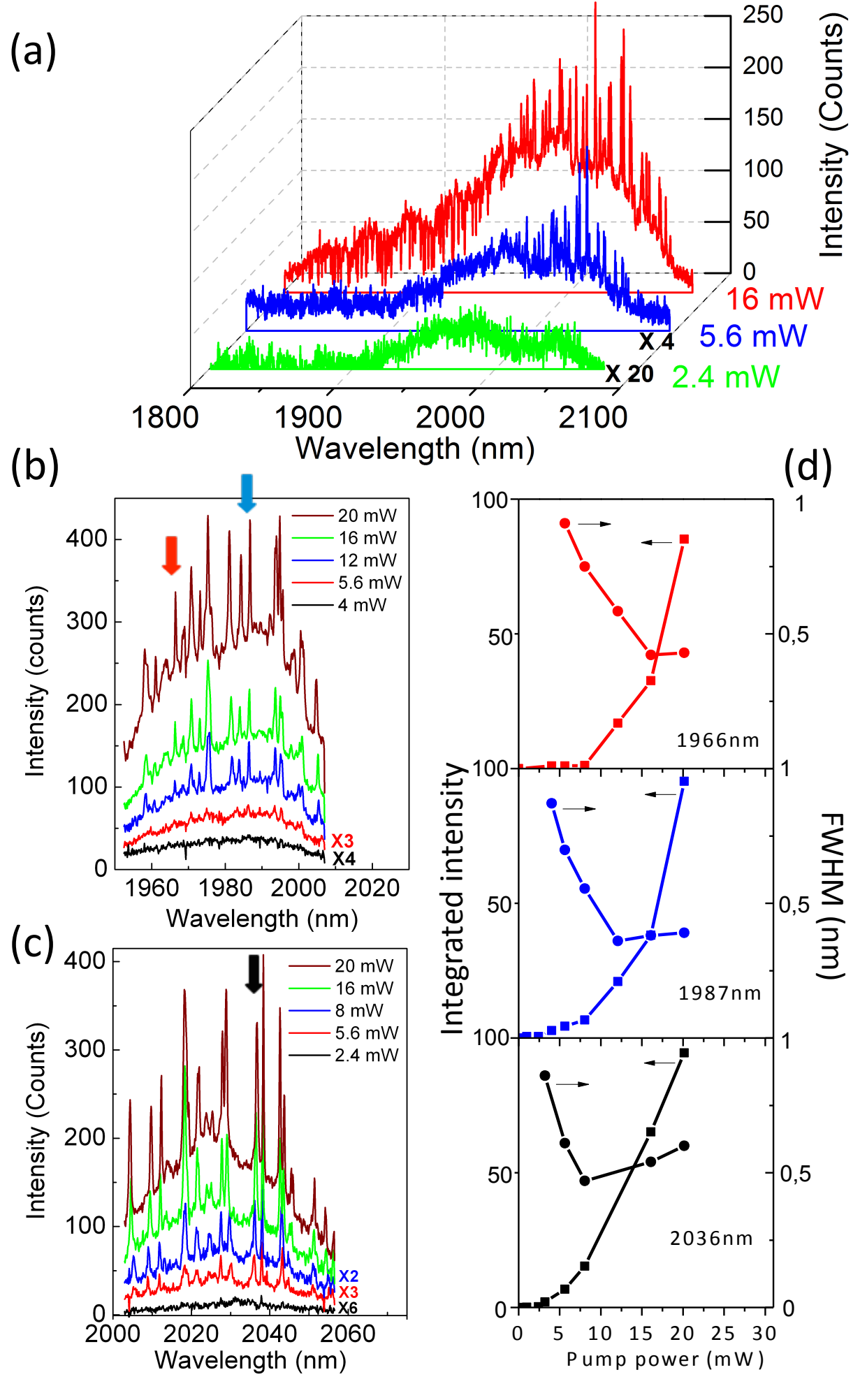
a)

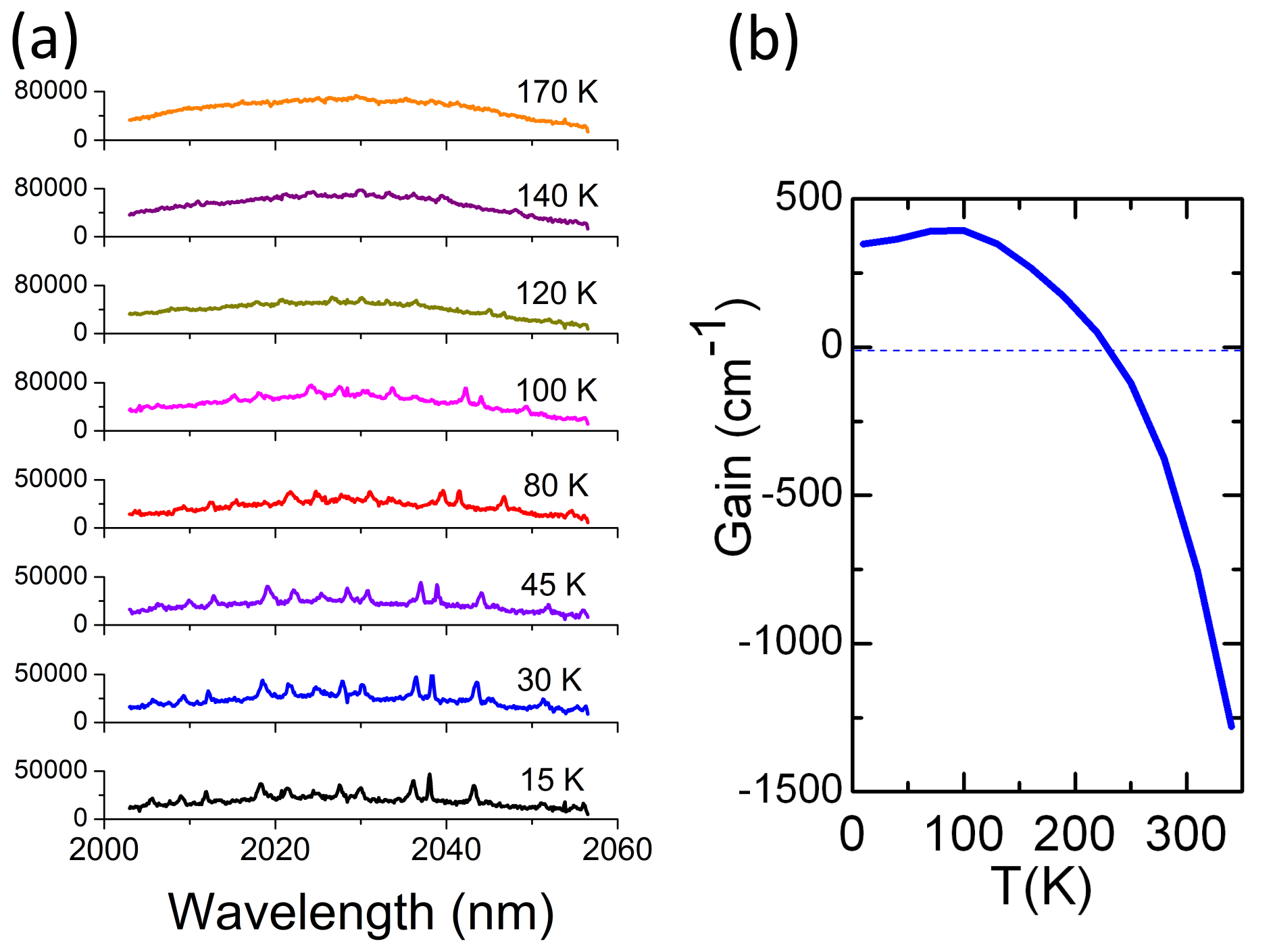

(1)
(2)
(3)
(4)
Silicon-on-Insulator
Germanium
SiN
Metal
Silicon

b)


Ge
Al
SiN
5 µm


(a)
Trace
0.02
0.01
0
0
2
4
6
Radius (μm)
(b)
0.07
0.05
0.03
0.01
-0.01
0
2
4
6
8
Radius (μm)
(c)
Maxi 326 K
250
150
50
Mini 15 K
SiO2
post
(d)
56 K
50
40
30
20
15 K
Al
post


(a)
Intensity (Counts)
250
200
150
100
50
0
16 mW
5.6 mW
2.4 mW
X 4
X 20
1800
1900
2000
2100
Wavelength (nm)
(b)
Intensity (counts)
400
300
200
100
0
20 mW
16 mW
12 mW
5.6 mW
4 mW
X3
X4
1960
1980
2000
2020
Wavelength (nm)
(c)
Intensity (Counts)
400
300
200
100
0
20 mW
16 mW
8 mW
5.6 mW
2.4 mW
X2
X3
X6
2000
2020
2040
2060
Wavelength (nm)
(d)
Integrated intensity
FWHM (nm)
100
50
1
0,5
1966nm
1987nm
2036nm
0
5
10
15
20
25
30
Pump power (mW)


(a)
80000
0
170 K
80000
0
140 K
80000
0
120 K
80000
0
100 K
50000
0
80 K
50000
0
45 K
50000
0
30 K
50000
0
15 K
2000
2020
2040
2060
Wavelength (nm)
(b)
500
0
-500
-1000
-1500
Gain (cm-1)
0
100
200
300
T(K)